scientific reports

Check for updates

OPEN

Increasing model resolution improves but overestimates global mid-depth circulation simulation

Haihong Guo[1,2,3], Zhaohui Chen[1,2]✉, Ruichen Zhu[1,2,3] & Jinzhuo Cai[1,2]

Increasing the spatial resolution in climate models has significantly improved the simulation of global upper-layer ocean circulation. However, the ability of high-resolution models to accurately reproduce mid-depth circulation, in terms of strength and direction, still remains uncertain. An analysis of 17 climate models with varying resolutions reveals that both low and high-resolution models depict weaker current speeds compared with observations. High-resolution models demonstrate improved simulations of current speed and flow direction, except in the Southern Ocean. The performance of high-resolution models in regions with strong currents is generally better than in regions with weak flows. Dynamically, increasing the model resolution enhances the representation of temporal variations in mid-depth circulation by effectively capturing mesoscale processes. However, this also results in an overestimation of their intensity by approximately 65% on average across the global ocean.

Ocean circulation is crucial for transporting heat and mass on regional and global scales, driving the exchange of mass and energy across the planet[1]. The circulation of the upper layer, particularly its large-scale processes, has been extensively investigated and is now well understood through theories, observations, and numerical models[2–4]. In the past three decades, advancements in satellite altimeter technology have bolstered our comprehension of the surface circulation in the global oceans[5].

However, due to the scarcity of observations, our understanding of mid-depth circulation remains largely unclear[6]. The mid-depth circulation (typically around 1000 m deep) is a critical zone which plays a vital role in maintaining the mass and energy balance of the global ocean[7]. Unlike the upper layer circulation, which is mainly driven by winds, the circulation in the deep ocean is influenced by both wind-driven and thermohaline processes[1]. Additionally, mid-depth circulation may be affected by bottom topography and remote baroclinic forcing due to its proximity to the seafloor[8,9]. Therefore, the dynamics of mid-depth circulation are even more complex than those in the upper layer, requiring further clarification.

Directly measuring mid-depth circulation is challenging and costly, leading to limited availability of in-situ observations[9]. Additionally, most previous observational studies primarily focus on regional variabilities, such as the energetic western boundary regions[10,11], without providing a comprehensive picture of mid-depth circulation in global oceans. Fortunately, the advent of the profiling floats and the implementation of the Argo program has been immensely beneficial for studying global subsurface ocean. Argo floats provide valuable temperature and salinity data that enhance the accuracy of ocean state analyses and improve seasonal forecast skill[12]. These data help reveal deep circulation, improve understanding of ocean eddies and mixing, highlight long-term ocean variability, quantify sea level rise contributions, and enhance weather predictions[13].

By 2020, Argo floats have provided an extensive dataset of approximately 2.4 million profiles. These profiles include temperature, salinity, and position data, covering the upper 2000 m of the ocean[13], which have significantly enhanced our understanding of the ocean interior. The Argo float trajectory can be utilized to estimate subsurface absolute velocities by considering its drift distance at the parking depth and the drifting duration[14]. Using this method, mid-depth circulations in regional and global oceans have been estimated in numerous studies[7,15–17]. Using over 1.3 million velocity estimates, the Scripps Institution of Oceanography has developed and continues to maintain a time-mean global velocity dataset for the 800–1200 dbar range[18] (see 'Argo Observations' in Methods). This dataset could serve as an effective benchmark for evaluating numerical models and reanalysis products regarding the global mid-depth circulation.

[1]Frontier Science Center for Deep Ocean Multispheres and Earth System (FDOMES) and Physical Oceanography Laboratory, Ocean University of China, 238 Songling Road, Qingdao 266100, China. [2]Laboratory for Ocean Dynamics and Climate, Qingdao Marine Science and Technology Center, Qingdao, China. [3]Laoshan Laboratory, Qingdao, China. ✉email: chenzhaohui@ouc.edu.cn

In addition to observations, numerical models provide another effective way to depict the mid-depth circulations globally[19]. The design and distribution of the Coupled Model Intercomparison Project Phase 6 (CMIP6) have made notable contributions to marine science[20]. The ocean, being a vital component of these climate models, has been well reproduced with increased model resolutions, particularly in terms of simulating the circulation patterns in the upper ocean. Compared to non-eddy-permitting models, high-resolution (0.25° or 0.1°) simulations from the High-Resolution Model Intercomparison Project (HighResMIP) allow for resolving some mesoscale processes, leading to enhanced simulations of the ocean's structure, variability, and long-term trends[21,22]. Increasing the resolution of climate models enhances their ability to represent upper ocean circulation by resolving the Rossby deformation radius[23,24]. The high-resolution model demonstrates advantages in explicitly representing mesoscale eddies and narrow boundary currents[25]. How these features are represented affects both the ocean's mean state and climate variability, including future climate response[26]. In addition, increasing resolution could help address bias issues in certain regions, such as the Atlantic[27]. However, the performance of increased resolution models in simulating mid-depth flow remains unclear. It is reported that model representations of global mid-depth circulation are compromised by inaccuracies in magnitude and direction[7]. Only 3.8% of mid-depth oceans are accurately modeled, while other regions show significant underestimations in current velocity. Ocean circulation is better understood in low-latitude regions but is notably poor in high latitudes, affecting predictions of currents, temperature, CO_2 sequestration, and sea-level rise[7].

Thus, to gain a better understanding of mid-depth circulation, it is beneficial to quantify the improvements offered by high-resolution models (see 'Climate models' in Methods). Here, we employ the Scripps Argo trajectory-based velocity product to assess the performance of both low and high-resolution CMIP6 models in representing mid-depth circulation. We use Spearman's rank correlation to evaluate current speed, cosine similarity to evaluate flow direction, and standard deviation to evaluate variations (see 'Data analysis method' in Methods). These evaluations seek to ascertain the efficacy of increasing the resolution of climate models as a valuable approach for accurately simulating the mid-depth circulation in global oceans.

Overview of the simulated global mid-depth circulation

To gain a comprehensive understanding of simulated mid-depth circulation and its ability to reproduce Argo observations, we first examine the spatial structure and global mean of mid-depth circulation and evaluate the performance of both low-resolution (LR) and high-resolution (HR) models (Fig. 1). The modeled velocities are obtained from the ensemble mean of multiple climate models in both LR and HR simulations. Regarding current speed, both the LR and HR simulations exhibit weaker amplitude compared to the observations, with a global mean of 0.013 m/s and 0.016 m/s for the LR and HR simulations, respectively, whereas the Argo product shows a global mean current speed of 0.019 m/s. The primary discrepancies are observed in the western boundary current (WBC) regions and the Antarctic Circumpolar Current (ACC) region (Fig. S1), characterized by high velocities (Fig. 1a,b). Another notable inconsistent region is the tropics, characterized by complex undercurrent systems,

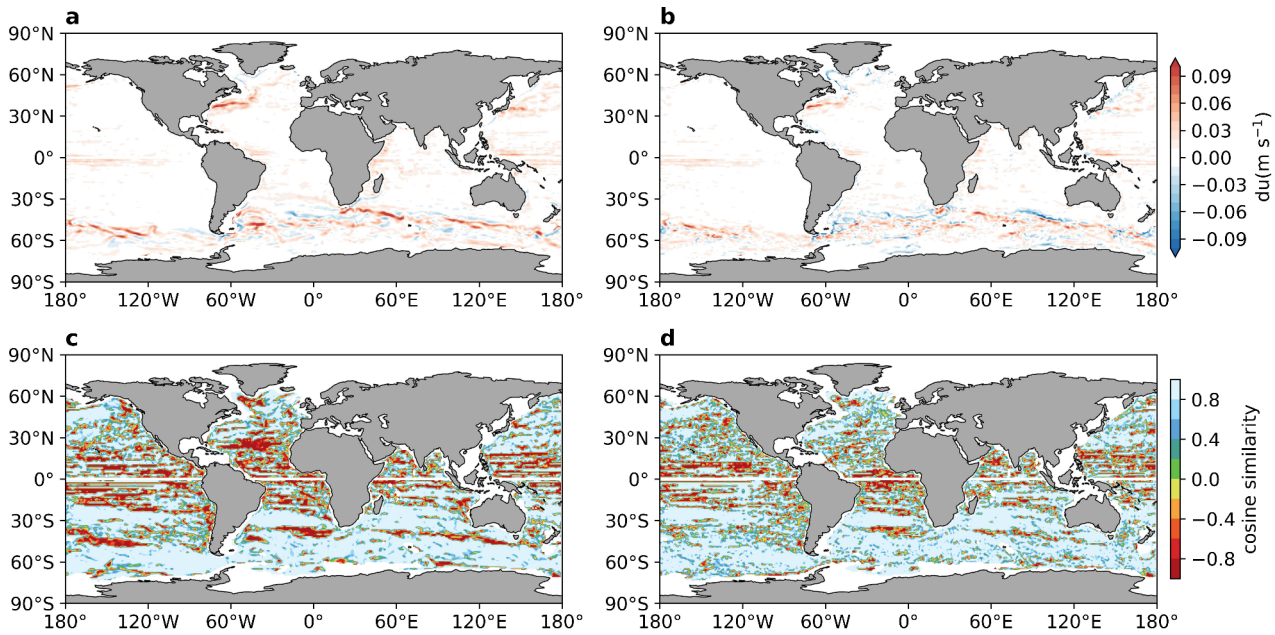

Fig. 1. Long-term mean velocity difference between models and Argo observations. (**a**,**b**), Differences in current speed (Argo minus Model) between the ensemble mean of models and the Argo observations in the LR (**a**) and HR (**b**) simulations. (**c**,**d**) Same as (**a**,**b**), but for cosine similarity. The map is created with Python 3.10.14 (https://www.python.org/downloads/release/python-31014/). Increasing model resolution improves both current speed and flow direction simulations.

where both HR and LR simulations exhibit relatively weak flows. The HR simulation exhibits improvements in the WBCs and their extension regions, such as the Kuroshio Current and the Gulf Stream. Nevertheless, the modeled flow in these regions remains weaker compared to the Argo observations. Moreover, in the ACC region, which is characterized by rich eddy activities, the increased resolution introduces greater complexity to the spatial structure of current differences.

Compared to the modeled current speeds, climate models show more limitations in simulating the flow direction of mid-depth circulations, especially in ocean interiors characterized by weak flow, where the modeled flow direction can even be reversed (Fig. 1c,d). In LR simulations, these reversed flow patterns are observed in certain low-latitude areas, such as the tropical Pacific and Atlantic (Fig. 1c). HR simulations notably enhance the modeled flow direction in these regions, particularly in the South Pacific and the North Atlantic (Fig. 1d). In comparison, both the LR and HR models demonstrate a reasonable representation of flow direction in the WBC regions and the ACC region.

It is noteworthy that the modeled flow direction in high-latitude regions is better than that in low-latitude regions. This difference is due to the ocean being more barotropic at higher latitudes, resulting from weaker stratification[28]. In high-latitude regions, weak oceanic stratification leads to the first baroclinic normal mode playing a dominant role[1]. In tropical regions, characterized by strong stratification, higher baroclinic modes are also important[29]. Consequently, the mid-depth circulation in high-latitude regions is more influenced by wind-driven processes compared to low-latitude regions. For instance, in the high-latitude North Pacific, such as the frontal regions in the Kuroshio and Oyashio Extensions, the wind-driven circulation in the upper ocean can extend downward to a depth of 1500 m[30,31]. In contrast, in the low-latitude Pacific, such as the North Equatorial Current and Countercurrent region, the wind-driven circulation remains confined to the upper 400–600 m[32]. Driven by the convergence of potential vorticity fluxes induced by eddies, abundant undercurrents exist beneath the thermocline in tropical oceans, where the mid-depth circulation deviates from—and can even be opposite to—the wind-driven circulation in the upper layer[33,34]. The presence of these undercurrents poses a significant challenge in accurately simulating mid-depth circulation in tropical regions. In addition, notable discrepancies in the LR simulations are observed along the northern edge of the ACC (Fig. 1c). However, these inconsistencies are noticeably mitigated in HR simulations, indicating that higher resolutions lead to a more accurate depiction of the ACC.

To conduct a more comprehensive evaluation of model performance across different latitudes, we calculated zonally averaged global current speed differences and cosine similarities (Fig. 2). The Argo observations indicate stronger current speeds compared to both the HR and LR models across most latitudes. The speed discrepancies are primarily concentrated in tropical and high-latitude regions, with HR models showing smaller differences compared to LR models (Fig. 2a). There are significant differences in the mid-latitudes around 40°N, primarily due to the inaccurate simulation of the downstream Gulf Stream (Fig. 1a,b), which can exceed model simulations by up to 70%[7]. Another significant difference occurs around 60°N, where the model produces stronger current speeds than observations. These discrepancies are primarily located in the North Atlantic region, especially the Labrador Sea. Although climate models could well reproduce the Atlantic Meridional Overturning Circulation, a large spread among models persists[27]. A more accurate representation of the Atlantic Ocean is still needed to improve the reliability of climate models. In subtropical areas, both HR and LR models exhibit similarly favorable performance. Regarding flow direction, both models effectively capture high-latitude flow, while large discrepancies emerge in tropical regions (Fig. 2b). Improvements in the HR models are limited across most latitudes; however, a distinct enhancement is evident within the ACC region.

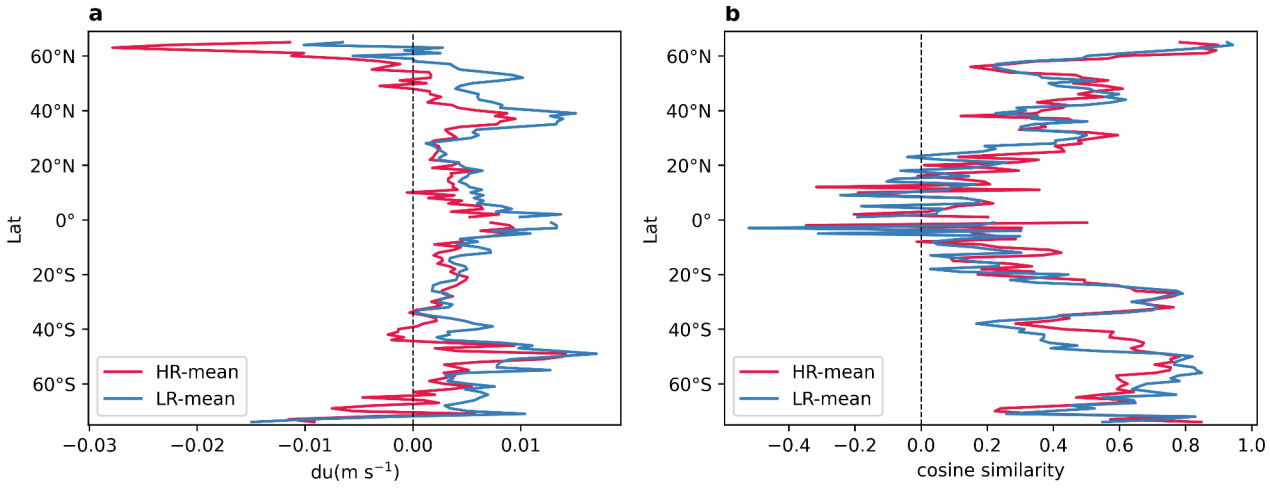

Fig. 2. Zonally averaged global current differences between models and observations. (**a**,**b**) Zonally averaged current speed differences (Argo minus Model) (**a**) and cosine similarity (**b**) between models and Argo observations in the HR (red) and LR (blue) models. The model's performance for both current and flow direction is latitude-dependent.

Model performance in different oceans

The performance of both LR and HR models varies across different regions. Therefore, we conducted evaluations across the Pacific Ocean, Atlantic Ocean, and Indian Ocean (three oceans), as well as examinations of tropical regions using a 30° latitudinal band centered around the equator, and the Southern Ocean. Compared to LR models, HR models consistently produce more accurate simulations in terms of both current speed and flow direction across most of these regions (Table 1).

In the three oceans, the HR models exhibit enhancements in current speed, with improvements ranging from 8 to 15%, accompanied by a reduced model spread. Specifically, model performance in the Atlantic Ocean is better than in the other two oceans. In the tropical oceans, both HR and LR models exhibit limitations in simulating current speed, with the largest model spread reaching 16% of the average. In the Southern Ocean, the modeled current speed shows better performance than in other regions for both HR and LR models. However, increased resolution weakens model performance in this region and introduces more uncertainties.

Regarding flow direction, HR models show improvements in both the Pacific and Atlantic Oceans. Despite the improvement, the Atlantic Ocean demonstrates poor performance in both HR and LR models in the extratropical regions. The Indian Ocean exhibits the best performance among the three oceans in both LR and HR models, with no improvements in the HR models. Similar to current speed, flow direction in tropical oceans is not convincingly reproduced, showing the lowest level of consistency. In the Southern Ocean, flow direction exhibits its best performance across the global oceans but is weakened in HR models. Although HR models generally show better performance in most areas, increased resolution consistently results in an expanded model spread (Table 1).

To further evaluate model performance in regional oceans and their differences, we divided the global ocean into several regions (Fig. S1 in Supporting Information). In general, these regions can be classified into two categories based on the strength of circulation: the subtropical WBC regions and the ACC region (red geometries in Fig. S1), characterized by strong flow, and the ocean interior and tropical regions (blue geometries in Fig. S1), characterized by weak flows. The WBC regions include the Kuroshio Current (KC), the Gulf Stream (GS), the Agulhas Current (AC), the East Australian Current (EAC), and the Brazil Current (BC). Meanwhile, the interior regions comprise the North Pacific (NP), the North Atlantic (NA), the South Indian (SI), the South Pacific (SP), and the South Atlantic (SA). Notably, the ACC region selected in this study differs from the Southern Ocean region, encompassing a confined band between 60°S and 40°S rather than spanning the entire Southern Ocean. This distinction is made to focus on the strong current region. The WBC and ACC regions are known for their abundance of eddies[35], contributing to more turbulent flows, while the interior regions are comparatively "calm". However, the narrow axes and rich mesoscale processes of WBCs present a challenge for coarse-resolution models in accurately representing their features. Therefore, it is beneficial to examine model performance in these different regions, respectively.

The modeled current speed in HR simulations has shown improvement compared to LR simulations in all WBC regions, especially for the Kuroshio Current and the Gulf Stream (Fig. 3a). Both LR and HR simulations exhibit a good representation of the ACC region, with negligible differences observed between them. However, in ocean interiors, the performance of HR models in simulating current speed varies by region (Fig. 3b). In the Atlantic interiors and tropical regions, increased resolution proves advantageous for simulating current speed, whereas it is less beneficial in the Pacific and South Indian regions. In general, the disparities between LR and HR simulations are smaller in ocean interiors compared to the WBC regions.

For flow direction, the performance of climate models with different resolutions exhibits a pattern similar to current speed (Fig. 3c,d). Although the improvement in flow direction is only moderate compared to that in current speed, HR simulations still outperform LR simulations in all WBC regions. Specifically, the East Australian Current region shows the largest improvement, while the other WBC regions display relatively weaker enhancements with increased resolution (Fig. 3c). In ocean interiors, the impact of increased resolution on flow direction generally aligns with that on current speed, except in the South Atlantic region, where LR simulations outperform HR simulations (Fig. 3d). However, the differences between LR and HR models in simulating flow direction are minimal in most ocean interiors. It is worth noting that the North Atlantic region exhibits the largest inconsistencies in the flow direction simulation (Figs. 1c and 3d). Despite limited improvements, HR simulations consistently enhance the modeled flow direction in this region, indicating a more accurate representation of the North Atlantic circulation (Fig. 3d).

	Spearman correlation		Cosine similarity	
Region	LR	HR	LR	HR
Pacific Ocean	0.35 ± 0.04	0.38 ± 0.03	0.23 ± 0.02	0.24 ± 0.01
Atlantic Ocean	0.53 ± 0.03	0.61 ± 0.02	0.17 ± 0.02	0.25 ± 0.04
Indian Ocean	0.42 ± 0.03	0.48 ± 0.03	0.39 ± 0.03	0.39 ± 0.06
Tropic Oceans	0.31 ± 0.05	0.33 ± 0.05	0.04 ± 0.03	0.11 ± 0.05
Southern Ocean	0.69 ± 0.04	0.65 ± 0.05	0.58 ± 0.02	0.54 ± 0.04

Table 1. Spearman correlation, cosine similarity, and their intermodel standard deviation for different regions in both HR and LR models. These values are calculated individually for each model and then averaged. All mean values in this table are statistically significant at the 95% confidence level. The HR models show improvements in most regions.

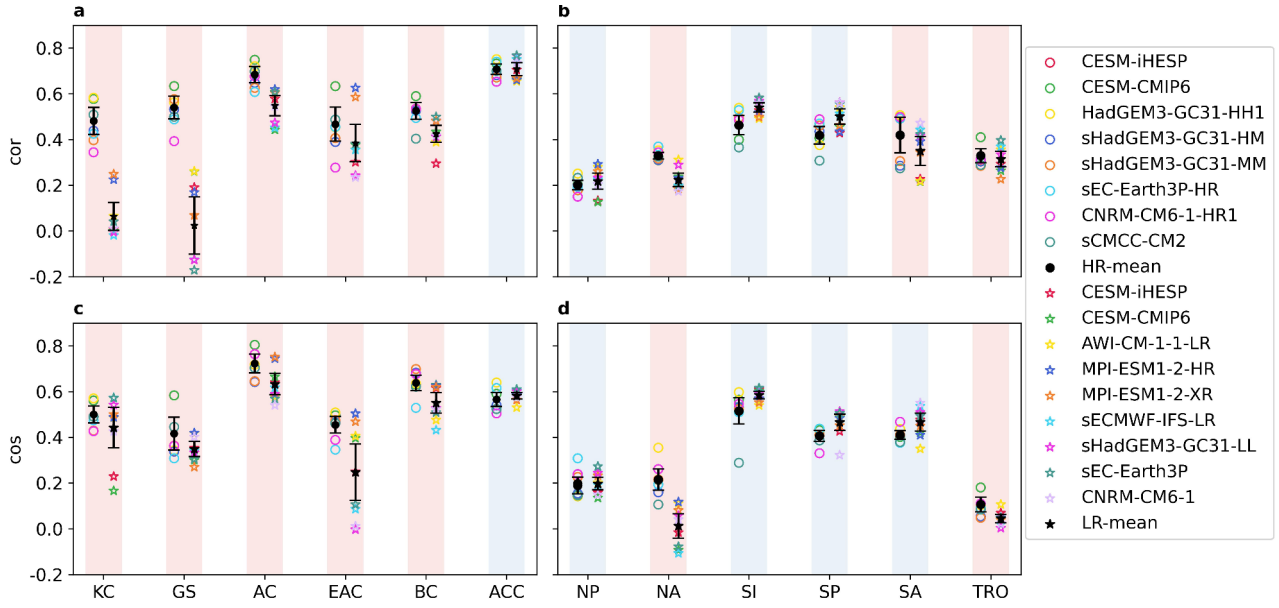

Fig. 3. Comparison of velocity between models and observations in different regions. (**a**–**d**) Spearman's rank correlation (**a**,**b**) and spatial-mean cosine similarity (**c**,**d**) in WBC and ACC regions (**a**,**c**), as well as in ocean interior and tropical regions (**b**,**d**). The colored circles (stars) represent HR (LR) simulations. The black symbols indicate the multi-model mean, while the error bars represent the 95% confidence intervals, estimated using a bootstrap method. The presence of red (blue) shading indicates that HR simulations outperform (underperform) LR simulations. Increasing model resolution consistently improves current speed but has varying effects on flow direction.

Overall, HR simulations exhibit better performance in the WBC regions than LR simulations for both current speed and flow direction (Fig. 3). This finding may initially seem counterintuitive, as the WBC regions exhibit the largest inconsistencies in current speed (Fig. 1a,b). However, this can be attributed to the fact that the mean strength of currents in these regions is typically stronger than in the ocean interiors. As a result, the relative differences become smaller in areas with stronger flow.

Improved but overestimated eddy processes in HR simulations

One of the most important advantages of increased resolution in numerical models is the more accurate simulation of the mesoscale eddy field[36,37]. As the first baroclinic Rossby deformation radius decreases from approximately 240 km in the near-equatorial band to less than 10 km at latitudes higher than about 60°[38], the coarse resolution (~ 1°) of LR simulations restricts their ability to effectively reproduce the eddy field. Fortunately, the increased resolution in HR simulations improves the ability of numerical models to resolve these mesoscale variabilities[21]. Although the Argo trajectory-based velocity product may not accurately depict the eddy variability for any specific period, we can utilize the velocity standard deviation (VSTD) derived from the time-varying, small-scale mapped estimate as an indicator of the strength of eddy processes[18]. The modeled VSTD is calculated from the monthly mean horizontal velocity data for the historical period. Although this time resolution is relatively coarse, making it difficult to resolve all eddy processes, the Argo-based VSTD is also insufficient for capturing the full extent of these processes. The purpose of using VSTD is not to quantify eddy activity directly but rather to serve as a proxy for the time variability.

The global spatial pattern of the modeled VSTD generally matches Argo observations. The Argo observes large VSTD in the WBC and ACC regions (Fig. 4b,e). Additionally, the zonal VSTD in tropical regions is notably high (Fig. 4b). However, the strength of the VSTD varies with model resolution. In LR simulations, the VSTD appears weaker compared to the Argo observations, particularly in the WBC regions, where it is distinctly lower than the Argo observations (Fig. 4f). In HR simulations, there is a considerable improvement in the VSTD (Fig. 4a,d). However, the strength of the VSTD in HR simulations is stronger than observed by Argo, suggesting an overestimation of the eddy field. An overestimation at a specific scale implies an underestimation of other processes, such as the subgrid scale, leading to biases in the energy cascade across different scales. Given the wide range of scales and complex interactions in ocean turbulence, enhancing the accuracy of subgrid-scale parameterizations is crucial for future climate models.

To quantify the modeled VSTD in climate models, we use linear regression to compare it with the observed VSTD. In LR simulations, the linear regression slopes for zonal and meridional VSTD are 0.53 and 0.51, respectively (Fig. 4g,h), with corresponding R^2 values of 0.81 and 0.75. These relatively lower slopes indicate an underestimation of VSTD in the LR simulations. By contrast, HR simulations exhibit steeper linear regression slopes for zonal and meridional VSTD, measuring 1.64 and 1.70, respectively (Fig. 4g,h), with R^2 values of 0.85 and 0.83. The HR simulations improve the underestimated VSTD seen in the LR simulations, however, they also

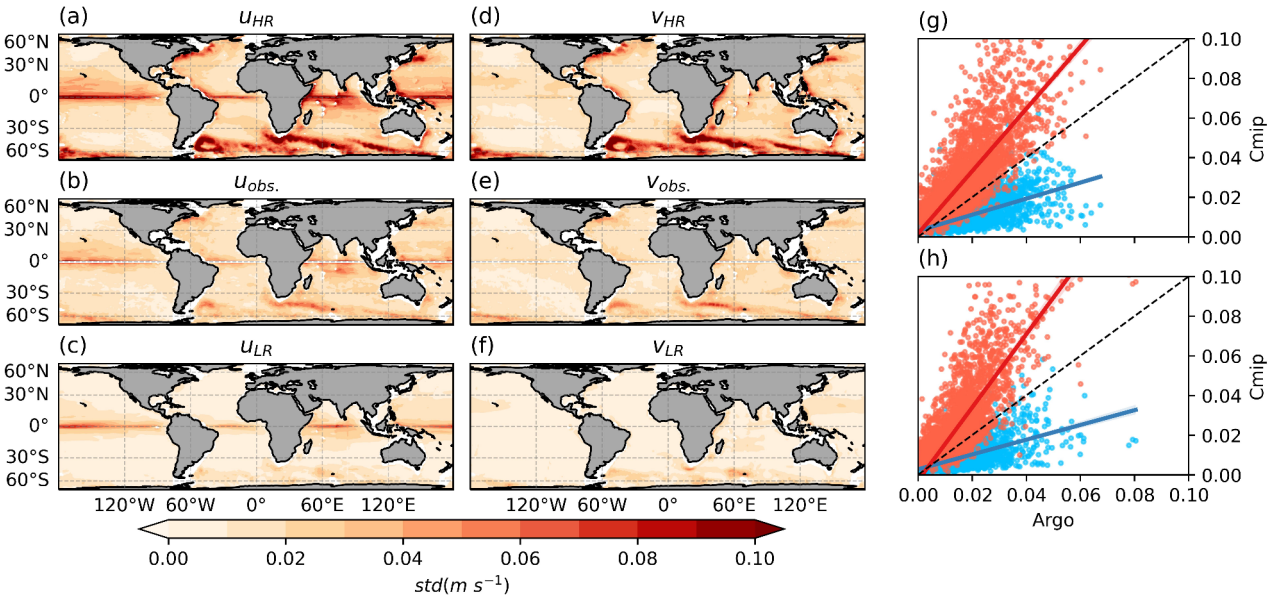

Fig. 4. The VSTD in models and observations. (**a**–**f**) The standard deviation of zonal (**a**–**c**) and meridional (**d**–**f**) velocities in the ensemble mean of HR models (**a**,**d**), the Argo observations (**b** and **e**), and the ensemble mean of LR models (**c**,**f**). (**g**,**h**) Scatterplots of the zonal (**g**) and meridional (**h**) VSTD between the Argo observations and the ensemble mean of models. The red (blue) symbols represent the HR (LR) models. The colored lines show the linear regression, with shading for the 95% confidence level. The black dashed line is the one-to-one reference. The map is created with Python 3.10.14 (https://www.python.org/downloads/release/python-31014/). The observed VSTD is stronger than in LR simulations but weaker than in HR simulations.

introduce excessive variance. Specifically, the LR simulations underestimate approximately 50% of the observed VSTD, while the HR simulations overestimate it by around 65%. Thus, the overestimation in the HR simulations is even greater than the underestimation in the LR simulations. The large amplitude of overestimation occurs in the eddy-rich regions (Fig. 4a,d), consistent with previous studies[39]. The overestimation may be attributed to coherent mesoscale eddies' intensity, which produces biases in the eddy growth stage[39]. Thus, an improved representation of eddies is needed in the next generation of climate models.

To gain further insights into the main sources of the VSTD differences, we conducted a more detailed examination of the VSTD in different regions (Fig. 5). The regional mean VSTD observed by Argo is stronger than that of the LR simulations but weaker compared to the HR simulations, consistent with the horizontal distribution (Fig. 4). The zonal and meridional components of VSTD demonstrate comparable magnitudes in most regions. However, it is noteworthy that in tropical regions, both Argo and climate models exhibit a relatively weaker meridional VSTD compared to the zonal components (Fig. 5b). This characteristic aligns well with the banded zonal flow observed in these regions. In general, the enhanced and overestimated VSTD in HR simulations is approximately 1.5 to 2 times higher than that observed by Argo in most WBC and ACC regions (Fig. 5a). Notably, the modeled VSTD in the EAC region is comparable to the Argo observations, being only around 1.2 times higher than the Argo data. In the ocean interiors, the modeled VSTD in HR simulations closely matches the Argo observations, with only a slightly greater magnitude (Fig. 5b). Therefore, the uncertainties of VSTD in HR simulations primarily occur in the WBC and ACC regions, consistent with the patterns observed in mean velocity (Fig. 1a,b) and the previous study[7].

Conclusions

In this study, we utilize 17 climate models to evaluate the performance of HR simulations in capturing global mid-depth circulations, in comparison to LR simulations. The observed mid-depth velocity data is obtained from the Argo dataset. Overall, both LR and HR models depict weaker current speeds compared to the observations, with substantial differences concentrated in tropical and high-latitude regions. The disparities in flow direction are primarily located in tropical regions, with more favorable model performance observed in high-latitude regions.

The model performance evidently varies with regions. The HR models consistently yield enhanced simulations than the LR models in terms of both current speed and flow direction across most ocean basins. The tropical oceans pose the most greatest challenge for accurately simulating both current speed and direction, while the Southern Ocean attains heightened accuracy compared to other oceanic areas. Despite improved flow direction in most areas by the HR models, the heightened resolution consistently leads to an increased model spread in all regions.

The performance of increased resolution in the WBC and ACC regions is superior to that in ocean interiors and tropical regions. There is a significant enhancement in HR simulations for both current speed and flow direction across all major subtropical WBCs. However, the performance of HR simulations varies regionally

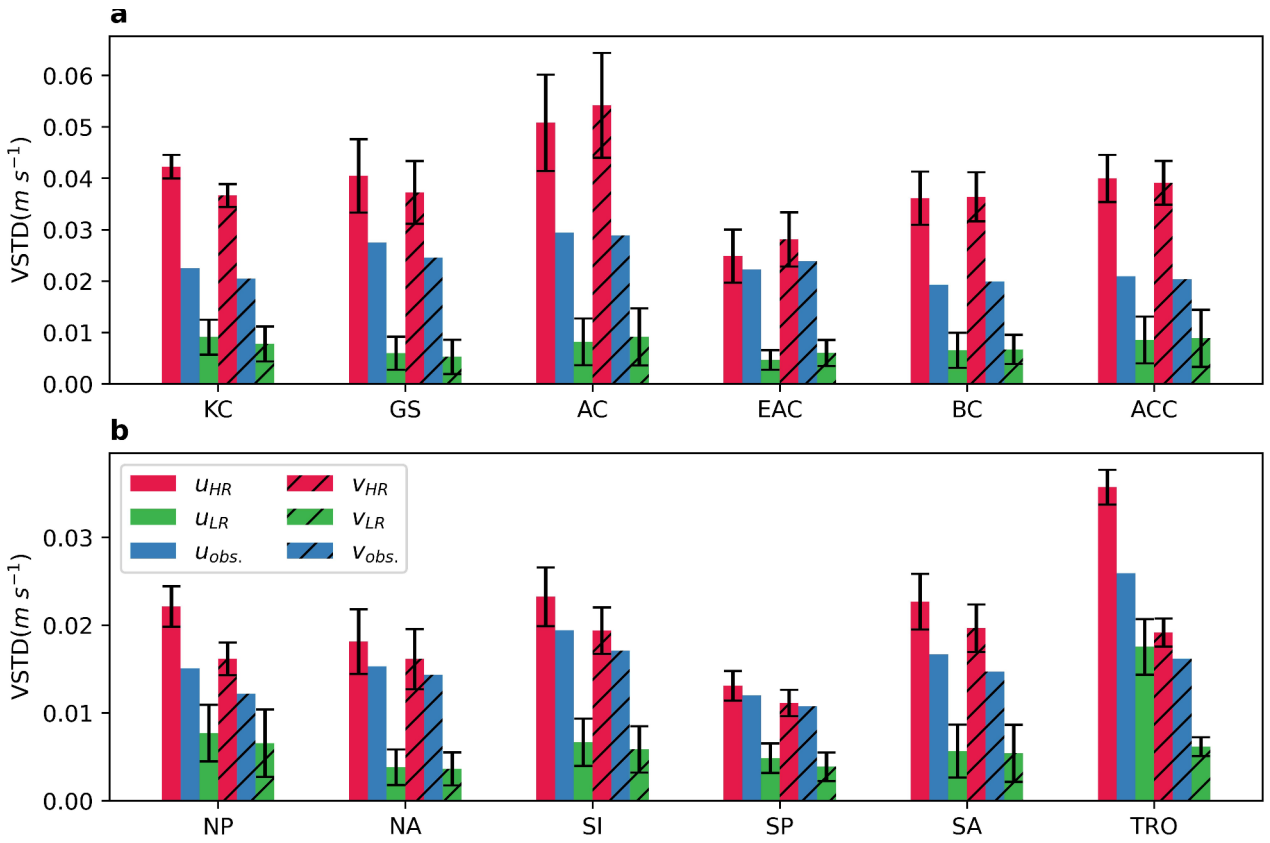

Fig. 5. Comparison of VSTD between models and observations in different regions. (**a**,**b**) The regional mean VSTD of zonal (solid-color patches) and meridional (line patches) components in the WBC and ACC regions (**a**), as well as in the ocean interior and tropical regions (**b**). The error bars represent the 95% confidence intervals, estimated using a bootstrap method. The enhanced simulation of VSTD in HR simulations primarily occurs in most WBC and ACC regions.

in ocean interiors. Both LR and HR simulations demonstrate limited representation of tropical flow direction, characterized by zonally banded jets. Furthermore, LR simulations underestimate mid-depth eddy processes, while HR simulations show improvements but tend to overestimate these processes. This improvement, yet overestimation, is primarily observed in the WBC and ACC regions. Our findings highlight the importance of reproducing global mid-depth circulations in climate models. On the one hand, assimilating more observed data, such as Argo floats, brings the model closer to representing the real ocean. On the other hand, improving parameterizations in climate models is crucial for accurately resolving more processes. This is crucial for advancing our understanding of mid-depth circulations and their role in the broader climate system.

Methods

Argo observations

A new subsurface velocity dataset, known as the Scripps Argo trajectory-based velocity product, has been provided by the Scripps Institution of Oceanography[18]. This dataset is derived from Core, BGC, and Deep Argo float trajectories collected from 2001 to 2020. When possible, extrapolated velocities were included, and transmitted velocities were used otherwise. The dataset utilizes a 1° horizontal resolution and incorporates over 1.3 million velocity estimations to reconstruct a time-mean velocity field for the 800–1200 dbar layer. To compute large-scale, time-invariant velocity estimation at each grid point, data within a 250 km radius were used, employing linear least squares fit to second-order polynomials that varied based on latitude and longitude[18].

Climate models

Based on the CMIP6 projects, eight low-resolution (LR) coupled climate models were assessed, and seven high-resolution (HR) models participating in HighResMIP were included for the comparison. The analysis focused on the "hist-1950" experiments conducted over the period 1950–2014. The sub-experiments with matching resolutions were averaged to one model product before use (Table S1 in Supporting Information). The eddy-free LR experiments were conducted at various horizontal resolutions ranging from 50 to 100 km in the ocean. By contrast, the HR experiments were conducted at different horizontal resolutions, including 25 km (eddy-present) and 10 km (eddy-rich) configurations. Additional model configurations are referred to as CESM[40], HadGEM3-GC3.1[41], EC-Earth3P[42], CMCC-CM2[43], CNRM-CM6-1[44], ECMWF-IFS[45], MPI-ESM1-2[46], AWI-CM-1-1[47].

Furthermore, a high-resolution simulation utilizing the Community Earth System Model version 1.3 developed by the International Laboratory for High-Resolution Earth System Prediction (CESM-iHESP)[40] is included in this study. This simulation incorporates historical forcing spanning from 1950 to 2005. To distinguish different CESM experiments, the CESM from CMIP6 is designated as CESM-CMIP6.

Detailed information about these climate models can be found in the Supporting Information (SI). The vertically-averaged horizontal velocity from 800 to 1200 m is chosen as a representation of the mid-depth circulation in all climate models. All the modeled velocity fields are resampled to a horizontal resolution of 1°, which is consistent with the horizontal resolution of the Argo velocity product. This resampling facilitates a direct comparison between the modeled and Argo velocity data.

Data analysis method

The modeled mid-depth circulation is evaluated by comparing the current speed, direction, and temporal variations between observations and models. First, Spearman's rank correlation analyses were utilized to examine the consistency in current speed between observations and models. This non-parametric method assesses the strength of the association between two ranked current speed. The Spearman's rank correlation is calculated using

$$r_s = \frac{\mathrm{cov}\left(R\left(u_o\right), R\left(u_m\right)\right)}{\sigma_R\left(u_o\right)\sigma_R\left(u_m\right)} \tag{1}$$

where $R(u_o)$ and $R(u_m)$ represent the ranks of the observed and modeled current speed, cov(R(u_o), R(u_m)) denotes the covariance of the rank variables, $\sigma_R(u_o)$ and $\sigma_R(u_m)$ indicate the standard deviations of the rank variables. The coefficient r_s ranges from −1 to 1. A positive (negative) value indicates a direct (inverse) monotonic relationship, while a value of 0 suggests no monotonic association between the variables.

To evaluate the modeled flow direction, cosine similarity is an effective measure of similarity between two non-zero vectors, which is defined as the cosine of the angle between them

$$\cos\left(\theta\right) = \frac{\mathrm{u_o} \cdot \mathrm{u_m}}{|\mathrm{u_o}|\,|\mathrm{u_m}|} \tag{2}$$

where u_o and u_m are the observed and modeled velocity vectors. It quantifies the similarity in direction between the two vectors. The cosine similarity value ranges from −1 to 1, where 1 indicates perfect similarity, -1 indicates perfect dissimilarity, and 0 indicates orthogonality between the vectors.

To assess the temporal variations of mid-depth circulation, we utilize the standard deviation (σ_u, σ_v) of horizontal velocities as an indicator, which can be computed by

$$\sigma_u^2 = \sum_{n=1}^{N} \frac{1}{N} u_n'^{\,2} \tag{3a}$$

$$\sigma_v^2 = \sum_{n=1}^{N} \frac{1}{N} u_v'^{\,2} \tag{3b}$$

where $u_n' = u_n - \bar{u}$ and $v_n' = v_n - \bar{v}$; u_n and v_n represent the zonal and meridional velocities, respectively, while $\bar{u}$ and $\bar{v}$ denote the mean velocities over the entire model period (N time steps). The standard deviation of observed velocities is calculated based on the time-varying, small-scale mapped estimate derived from the Argo velocity product[18]. It is worth noticing that there may be some discrepancies between the model and observations. On the one hand, the Argo-based temporal variations may not fully capture high-frequency variability due to the use of trajectories from 5- to 25-day cycles. In most areas of the global oceans, long-time cycles dominate. On the other hand, the Argo floats cannot provide continuous observations at a fixed position, further limiting the representation of high-frequency variations. To mitigate this limitation, we compute the temporal variation from the model using monthly mean velocities during the historical period of the climate models. Comparing the standard deviation of modeled and observed horizontal velocities provides a suitable estimation for assessing temporal variations of the mid-depth circulation.

Data availability

The CMIP6 model data, including the HighResMIP data, is available for download from the official Earth System Grid Federation (ESGF) website (https://esgf-node.llnl.gov/search/cmip6/). The CESM-iHESP data used in this work are available from the Texas A&M Datahub portal (https://ihesp.github.io/archive/products/ihesp-products/data-release/HIST_TNST/ocn/index.html). The Scripps Institution of Oceanography Argo velocity dataset is freely available on the UCSD library (https://doi.org/10.6075/J0KD1Z35), Argo website (https://argo.ucsd.edu/data/argo-data-products/velocity-products/).

Received: 14 August 2024; Accepted: 15 November 2024
Published online: 26 November 2024

References

1. Huang, R. X. *Ocean Circulation* (Cambridge University Press, 2009).
2. Stommel, H. The westward intensification of wind-driven ocean currents. *Trans. Am. Geophys. Union*. **29**, 202 (1948).

3. Schott, F. A. & Böning, C. W. The WOCE model in the western equatorial Atlantic: Upper layer circulation. *J. Geophys. Res.* **96**, 6993 (1991).
4. Rosati, A. & Miyakoda, K. A general circulation model for upper ocean simulation. *J. Phys. Oceanogr.* **18**, 1601–1626 (1988).
5. Ducet, N., Le Traon, P. Y. & Reverdin, G. Global high-resolution mapping of ocean circulation from TOPEX/poseidon and ERS-1 and -2. *J. Geophys. Res. Ocean.* **105**, 19477–19498 (2000).
6. Reid, J. L. On the mid-depth circulation of the world ocean. *Evol. Phys. Oceanogr.* **623**, 70–111 (1981).
7. Su, F. et al. Widespread global disparities between modelled and observed mid-depth ocean currents. *Nat. Commun.* **14**, 2089 (2023).
8. Käse, R. H., Biastoch, A. & Stammer, D. B. On the mid-depth circulation in the Labrador and Irminger seas. *Geophys. Res. Lett.* **28**, 3433–3436 (2001).
9. Bower, A. S. et al. Directly measured mid-depth circulation in the northeastern North Atlantic Ocean. *Nature* **419**, 603–607 (2002).
10. Pickart, R. S. & Smethie, W. M. How does the deep western boundary current cross the gulf stream? *J. Phys. Oceanogr.* **23**, 2602–2616 (1993).
11. Jayne, S. R. et al. The Kuroshio extension and its recirculation gyres. *Deep Res. Part. I Oceanogr. Res. Pap*. **56**, 2088–2099 (2009).
12. Balmaseda, M., Anderson, D. & Vidard, A. Impact of Argo on analyses of the global ocean. *Geophys. Res. Lett.* **34**, 1–6 (2007).
13. Johnson, G. C. et al. Argo-two decades: Global oceanography, revolutionized. *Ann. Rev. Mar. Sci.* **14**, 379–403 (2022).
14. Davis, R. E., Regier, L. A., Dufour, J. & Webb, D. C. The autonomous lagrangian circulation explorer (ALACE). *J. Atmos. Ocean. Technol.* **9**, 264–285 (1992).
15. Lavender, K. L., Owens, B., Davis, R. E. & W. & The mid-depth circulation of the subpolar North Atlantic Ocean as measured by subsurface floats. *Deep Res. Part. I Oceanogr. Res. Pap*. **52**, 767–785 (2005).
16. Xie, J. & Zhu, J. Estimation of the surface and mid-depth currents from Argo floats in the Pacific and error analysis. *J. Mar. Syst.* **73**, 61–75 (2008).
17. Ollitrault, M. & De Verdière, A. C. The ocean general circulation near 1000-m depth. *J. Phys. Oceanogr.* **44**, 384–409 (2014).
18. Zilberman, N. V., Scanderbeg, M., Gray, A. R. & Oke, P. R. Scripps Argo trajectory-based velocity product: Global estimates of absolute velocity derived from core, biogeochemical, and deep Argo float trajectories at parking depth. *J. Atmos. Ocean. Technol.* **40**, 361–374 (2023).
19. Brandt, P. & Eden, C. Annual cycle and interannual variability of the mid-depth tropical Atlantic Ocean. *Deep Sea Res. Part. I Oceanogr. Res. Pap*. **52**, 199–219 (2005).
20. Eyring, V. et al. Overview of the coupled model Intercomparison Project Phase 6 (CMIP6) experimental design and organization. *Geosci. Model. Dev.* **9**, 1937–1958 (2016).
21. Haarsma, R. J. et al. High resolution model intercomparison project (HighResMIP v1.0) for CMIP6. *Geosci. Model. Dev.* **9**, 4185–4208 (2016).
22. Fox-Kemper, B. et al. Challenges and prospects in ocean circulation models. *Front. Mar. Sci.* **6**, 1–29 (2019).
23. Hewitt, H. T. et al. The impact of resolving the Rossby radius at mid-latitudes in the ocean: Results from a high-resolution version of the Met Office GC2 coupled model. *Geosci. Model. Dev.* **9**, 3655–3670 (2016).
24. Chassignet, E. P. & Xu, X. On the importance of high-resolution in large-scale ocean models. *Adv. Atmos. Sci.* **38**, 1621–1634 (2021).
25. Hewitt, H. T. et al. Will high-resolution global ocean models benefit coupled predictions on short-range to climate timescales? *Ocean. Model.* **120**, 120–136 (2017).
26. Hewitt, H. T. et al. Resolving and parameterising the ocean mesoscale in earth system models. *Curr. Clim. Chang. Rep.* **6**, 137–152 (2020).
27. Weijer, W., Cheng, W., Garuba, O. A., Hu, A. & Nadiga, B. T. CMIP6 models predict significant 21st century decline of the Atlantic Meridional overturning circulation. *Geophys. Res. Lett.* **47**, (2020).
28. Vallis, G. K. *Atmospheric and Oceanic Fluid Dynamics: Fundamentals and Large-Scale Circulation* (Cambridge University Press, 2017).
29. Huang, K. et al. Baroclinic characteristics and energetics of annual rossby waves in the southern tropical Indian Ocean. *J. Phys. Oceanogr.* **50**, 2591–2607 (2020).
30. Halkin, D. & Rossby, T. The structure and transport of the Gulf Stream at 73°W. *J. Phys. Oceanogr.* **15**, 1439–1452 (1985).
31. Yoshikawa, Y., Church, J. A., Uchida, H. & White, N. J. Near bottom currents and their relation to the transport in the Kuroshio extension. *Geophys. Res. Lett.* **31**, 1–5 (2004).
32. Qiu, B., Nakano, T., Chen, S. & Klein, P. Submesoscale transition from geostrophic flows to internal waves in the northwestern Pacific upper ocean. *Nat. Commun.* **8**, 14055 (2017).
33. Stramma, L. & Schott, F. The mean flow field of the tropical Atlantic Ocean. *Deep Sea Res. Part. II Top. Stud. Oceanogr.* **46**, 279–303 (1999).
34. Johnson, G. C., Sloyan, B. M., Kessler, W. S. & McTaggart, K. E. Direct measurements of upper ocean currents and water properties across the tropical Pacific during the 1990s. *Prog Oceanogr.* **52**, 31–61 (2002).
35. Imawaki, S., Bower, A. S., Beal, L. & Qiu, B. Western boundary currents. In *International Geophysics* vol. 103 305–338 (Elsevier Ltd., 2013).
36. Kang, D. & Curchitser, E. N. Gulf Stream eddy characteristics in a high-resolution ocean model. *J. Geophys. Res. Ocean.* **118**, 4474–4487 (2013).
37. Rieck, J. K., Böning, C. W., Greatbatch, R. J. & Scheinert, M. Seasonal variability of eddy kinetic energy in a global high-resolution ocean model. *Geophys. Res. Lett.* **42**, 9379–9386 (2015).
38. Chelton, D. B., DeSzoeke, R. A., Schlax, M. G., Naggar, E. & Siwertz, N. Geographical variability of the first baroclinic rossby radius of deformation. *J. Phys. Oceanogr.* **28**, 433–460 (1998).
39. Ding, M. et al. Overestimated eddy kinetic energy in the eddy-rich regions simulated by eddy-resolving global ocean–sea ice models. *Geophys. Res. Lett.* **49**, (2022).
40. Chang, P. et al. An unprecedented set of high-resolution earth system simulations for understanding multiscale interactions in climate variability and change. *J. Adv. Model. Earth Syst.* **12**, 1591–1594 (2020).
41. Roberts, M. J. et al. Description of the resolution hierarchy of the global coupled HadGEM3-GC3.1 model as used in CMIP6 HighResMIP experiments. *Geosci. Model. Dev.* **12**, 4999–5028 (2019).
42. Haarsma, R. et al. HighResMIP versions of EC-Earth: EC-Earth3P and EC-Earth3P-HR - description, model computational performance and basic validation. *Geosci. Model. Dev.* **13**, 3507–3527 (2020).
43. Cherchi, A. et al. Global mean climate and main patterns of variability in the CMCC-CM2 coupled model. *J. Adv. Model. Earth Syst.* **11**, 185–209 (2019).
44. Voldoire, A. et al. Evaluation of CMIP6 DECK experiments with CNRM-CM6-1. *J. Adv. Model. Earth Syst.* **11**, 2177–2213 (2019).
45. Roberts, C. D. et al. Climate model configurations of the ecmwf integrated forecasting system (ecmwf-ifs cycle 43r1) for highresmip. *Geosci. Model. Dev.* **11**, 3681–3712 (2018).
46. Gutjahr, O. et al. Max planck institute earth system model (MPI-ESM1.2) for the high-resolution model intercomparison project (HighResMIP). *Geosci. Model. Dev.* **12**, 3241–3281 (2019).
47. Semmler, T. et al. Simulations for CMIP6 with the AWI climate model AWI-CM-1-1. *J. Adv. Model. Earth Syst.* **12**, 1–34 (2020).

Acknowledgements
This research is financially supported by the National Natural Science Foundation of China (42306023, 42225601, 42076009), the Fundamental Research Funds for the Central Universities (202072001), the Shandong Province Postdoctoral Program for Innovative Talents (SDBX2023033), and the China Postdoctoral Science Foundation (GZB20230690). Z. Chen is partly supported by the Taishan Scholar Funds (tsqn201812022). The authors extend our sincere thanks to thanks to Professor Alison Gray from the School of Oceanography, University of Washington, for generously providing the gridded Argo velocity data.

Author contributions
Haihong Guo: Methodology, Original draft preparation. Zhaohui Chen: Conceptualization, Supervision. Ruichen Zhu: Investigation. Jinzhuo Cai: Data curation.

Declarations

Competing interests
The authors declare no competing interests.

Additional information
Supplementary Information The online version contains supplementary material available at https://doi.org/10.1038/s41598-024-80152-4.

Correspondence and requests for materials should be addressed to Z.C.

Reprints and permissions information is available at www.nature.com/reprints.

Publisher's note Springer Nature remains neutral with regard to jurisdictional claims in published maps and institutional affiliations.

Terms and Conditions

Springer Nature journal content, brought to you courtesy of Springer Nature Customer Service Center GmbH (“Springer Nature”).
Springer Nature supports a reasonable amount of sharing of research papers by authors, subscribers and authorised users (“Users”), for small-scale personal, non-commercial use provided that all copyright, trade and service marks and other proprietary notices are maintained. By accessing, sharing, receiving or otherwise using the Springer Nature journal content you agree to these terms of use (“Terms”). For these purposes, Springer Nature considers academic use (by researchers and students) to be non-commercial.
These Terms are supplementary and will apply in addition to any applicable website terms and conditions, a relevant site licence or a personal subscription. These Terms will prevail over any conflict or ambiguity with regards to the relevant terms, a site licence or a personal subscription (to the extent of the conflict or ambiguity only). For Creative Commons-licensed articles, the terms of the Creative Commons license used will apply.
We collect and use personal data to provide access to the Springer Nature journal content. We may also use these personal data internally within ResearchGate and Springer Nature and as agreed share it, in an anonymised way, for purposes of tracking, analysis and reporting. We will not otherwise disclose your personal data outside the ResearchGate or the Springer Nature group of companies unless we have your permission as detailed in the Privacy Policy.
While Users may use the Springer Nature journal content for small scale, personal non-commercial use, it is important to note that Users may not:

1. use such content for the purpose of providing other users with access on a regular or large scale basis or as a means to circumvent access control;
2. use such content where to do so would be considered a criminal or statutory offence in any jurisdiction, or gives rise to civil liability, or is otherwise unlawful;
3. falsely or misleadingly imply or suggest endorsement, approval , sponsorship, or association unless explicitly agreed to by Springer Nature in writing;
4. use bots or other automated methods to access the content or redirect messages
5. override any security feature or exclusionary protocol; or
6. share the content in order to create substitute for Springer Nature products or services or a systematic database of Springer Nature journal content.

In line with the restriction against commercial use, Springer Nature does not permit the creation of a product or service that creates revenue, royalties, rent or income from our content or its inclusion as part of a paid for service or for other commercial gain. Springer Nature journal content cannot be used for inter-library loans and librarians may not upload Springer Nature journal content on a large scale into their, or any other, institutional repository.
These terms of use are reviewed regularly and may be amended at any time. Springer Nature is not obligated to publish any information or content on this website and may remove it or features or functionality at our sole discretion, at any time with or without notice. Springer Nature may revoke this licence to you at any time and remove access to any copies of the Springer Nature journal content which have been saved.
To the fullest extent permitted by law, Springer Nature makes no warranties, representations or guarantees to Users, either express or implied with respect to the Springer nature journal content and all parties disclaim and waive any implied warranties or warranties imposed by law, including merchantability or fitness for any particular purpose.
Please note that these rights do not automatically extend to content, data or other material published by Springer Nature that may be licensed from third parties.
If you would like to use or distribute our Springer Nature journal content to a wider audience or on a regular basis or in any other manner not expressly permitted by these Terms, please contact Springer Nature at

onlineservice@springernature.com